European Journal of Medicinal Chemistry 79 (2014) 399–412

Contents lists available at ScienceDirect

European Journal of Medicinal Chemistry

journal homepage: http://www.elsevier.com/locate/ejmech

Original article

Identification and optimization of novel Hsp90 inhibitors with tetrahydropyrido[4,3-d]pyrimidines core through shape-based screening

Hao-Peng Sun [a,b,c,1], Jian-Min Jia [a,b,1], Fen Jiang [a,b], Xiao-Li Xu [a,b], Fang Liu [a,b], Xiao-Ke Guo [a,b], Bahidja Cherfaoui [a,b], Hao-Ze Huang [a,b], Yang Pan [a,b], Qi-Dong You [a,b,*]

[a] Jiangsu Key Laboratory of Drug Design and Optimization, China Pharmaceutical University, Nanjing 210009, China
[b] State Key Laboratory of Natural Medicines, China Pharmaceutical University, Nanjing 210009, China
[c] Department of Medicinal Chemistry, School of Pharmacy, China Pharmaceutical University, Nanjing 210009, China

ARTICLE INFO

Article history:
Received 21 January 2014
Received in revised form
19 March 2014
Accepted 20 March 2014
Available online 21 March 2014

Keywords:
Hsp90 inhibitors
ROCS
Design and synthesis

ABSTRACT

Rapid Overlay of Chemical Structures (ROCS), which can rapidly identify potentially active compounds by shape comparison, is recognized as a powerful virtual screening tool. By ROCS, a class of novel Hsp90 inhibitors was identified. The calculated binding mode of the most potent hit **36** guided us to design and synthesize a series of analogs (**57a**–**57h**). Over 100-fold improvement was achieved in the target-based assay. The most potent compound **57h** inhibited Hsp90 with IC_{50} 0.10 ± 0.01 μM. It also showed much improved cell potency and ligand efficiency. Our study showed that ROCS is efficient in the identification of novel cores of Hsp90 inhibitors. **57h** can be ideal leads for further optimization.

1. Introduction

Molecular chaperones are protein machines that are responsible for conformational stability, maturation, and function of other substrate proteins, which are known as clients [1]. Many molecular chaperones and co-chaperones have been identified to date. Among all the molecular chaperones, a 90 kDa heat shock protein (Hsp90) is the most attractive member and the most extensively studied [2–5]. Hsp90 is a molecular chaperone whose association is required for the stability and function of multiple mutated, chimeric and over-expressed signaling proteins that promote cancer cell growth and/or survival [6–8]. Hsp90 client proteins include mutated signaling proteins (p53, Bcr-Abl, Raf-1, Akt, etc.), HER2/Neu (ErbB2), nNos, Src, Flt-3, hTert, c-Met, HIF-1α, epidermal growth factor receptors (EGFRs) and growth factor receptors (IGF-1Rs), Cdk4 [9]. Several Hsp90 clients are notorious oncogenes (Raf-1, Akt, Cdk4, Src, Flt-3, hTert, c-Met, etc.), and five of them are clinically validated cancer targets: HER-2/neu, Bcr-Abl, estrogen receptor, androgen receptor, and VEGFR [9–12]. Additionally, Hsp90 derived from tumor cells has particularly higher expression level (4%–6% of the whole proteomic load of the cell) than in normal cells (1%–2%), this makes Hsp90 to be an ideal and selective target in the treatment of cancers [13–17]. Besides, targeting Hsp90 leads to the regulation of multiple pathways simultaneously, therefore, it is a promising therapeutic strategy in the suppression of tumor acquiring resistance [18].

The Hsp90 protein folding process is ATP dependent. Chaperoning of these client proteins is regulated through a dynamic cycle driven by ATP binding to Hsp90 and subsequent hydrolysis [19]. Inhibition of the ATPase activity of Hsp90 disrupts an ongoing "folding" cycle, including multiple co-chaperone proteins, and in turn leads to the destabilization, ubiquitination, and ultimately proteasomal degradation of client proteins [20]. The identification of Hsp90 inhibitors has been attractive for medicinal chemists since the discovery of geldanamycin and radicicol (Fig. 1), which are able to inhibit Hsp90 function through binding to the ATP binding pocket in its N-terminal domain [21]. In 1998–1999, the first clinical trials with an Hsp90 inhibitor were initiated on the geldanamycin derivative 17-allylamino-17-desmethoxygeldanamycin (**17-AAG**, Fig. 1). Although with high *in vitro* activity, the poor solubility as well as the hepatotoxicity hinder the further usage of **17-AAG** as clinical candidate [22]. The water-soluble analog 17-dimethylaminoethylgeldanamycin (**17-DMAG**, Fig. 1), proves to be

* Corresponding author. Jiangsu Key Laboratory of Drug Design and Optimization, China Pharmaceutical University, Nanjing, 210009, China.
E-mail address: youqidong@gmail.com (Q.-D. You).
[1] These authors contributed equally to this work.

http://dx.doi.org/10.1016/j.ejmech.2014.03.061
0223-5234/

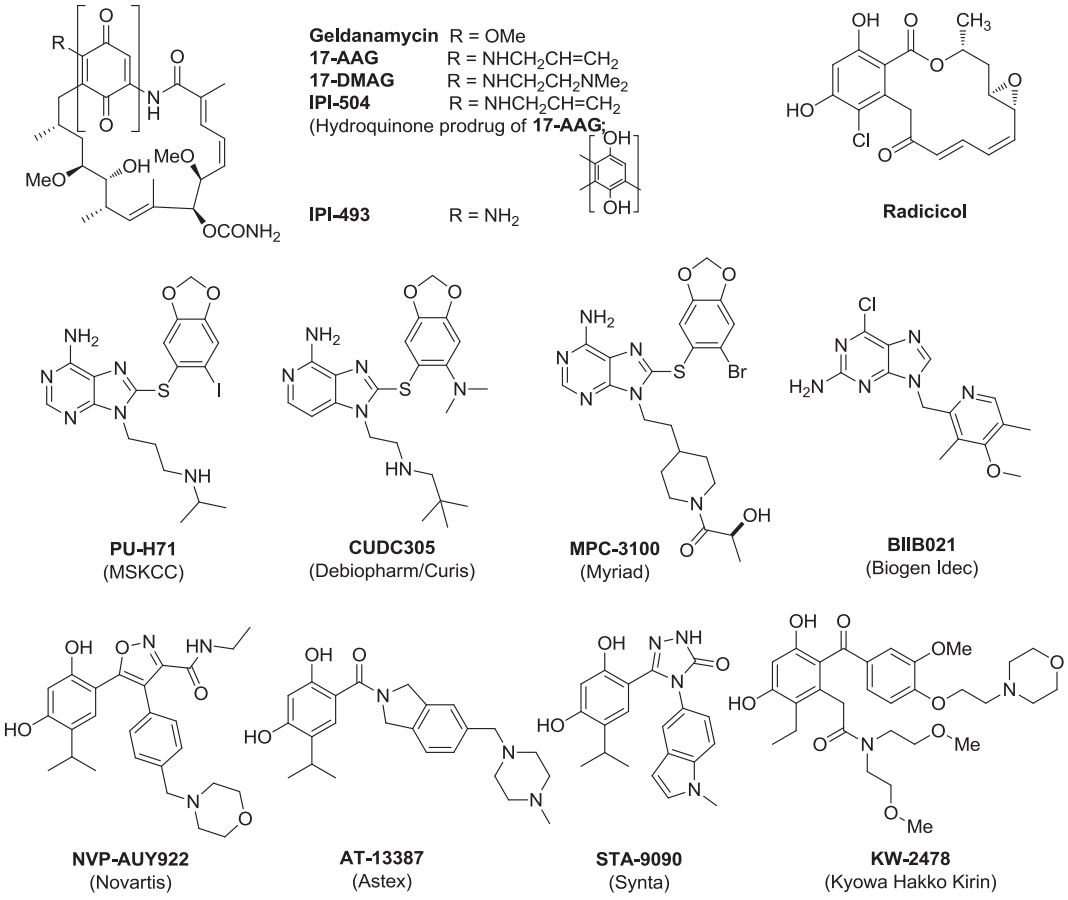

Fig. 1. Hsp90 inhibitors in clinical trials.

more toxic in preclinical species [23]. 17-AAG hydroquinone (**IPI-504**, Fig. 1) and its major metabolite 17-amino-17-desmethoxygeldanamycin (**17-AG**, Fig. 1) are now being developed by Infinity. They displayed good water solubility, much improved oral bioavailability [24,25].

In parallel, many fully synthetic small molecules are reported as potent and selective Hsp90 inhibitors by various institutions. Some of these compounds have entered into clinical trials in different phase [26,27]. Based on the structures of these small molecule inhibitors, there are two major cores, the purine and resorcinol. The purine class is designed by structural homology with ATP [28]. Many inhibitors belong to this family and among them, **PU-H71** (Memorial Sloan-Kettering Cancer Center, phase I) [29], **CUDC305** (Debiopharm, phase I) [30], **MPC-3100** (Myrexis, phase I) [31], **BIIB021** (Biogen Idec, phase II) (Fig. 1) are now in clinical trial [32]. The resorcinol scaffold is another important class of Hsp90 inhibitors, **NVP-AUY922** (Novartis, phase II) [33], **AT-13387** (Astex, phase II) [34], **STA-9090** (Synta, phase II) [35] and **KW-2478** (Kyowa Hakko Kirin, phase I/II) [36] are in clinical study. However, to date, no Hsp90 inhibitors can fully satisfy the requirement of safety and stability, thus none of them is approved to enter the market. As a result, efficient identification of promising inhibitors with different chemotypes is still a demanding task in this area.

Ligand-based virtual screening of large compound databases has been proved to an effective method in discovering hits with novel chemotypes [37–39]. It is also be widely agreed that ligand-based methods are more efficient and duplicable than structure-based methods. Among all the Ligand-based approaches, the qualitative (e.g. Hiphop model) [40] or quantitative (e.g. Hypogen model) [41] common structure pharmacophore might be the most successful and popular models. However, these methods are closely depend on the training set selection during the model construction. The resulted models always pay too much attentions on the common structural information, neglecting the unique characters of a given target, such as spatial volume requirements and physicochemical properties. Additionally, the experience of the researchers also deeply affects the accuracy and reliability of the models.

Rapid Overlay of Chemical Structures (ROCS) [42] is another useful ligand-based method that can avoid the problems mentioned above. It uses an alignment algorithm accounting shape/physicochemical properties for the query molecule orientation. The hits from this model not only have similar arrangement of critical chemical features to the reference molecule, but also possess similar molecular shape and orientation. The complement of these characters can help medicinal chemists to discover compounds which may very different to the reference molecule, but are actually very similar in the whole level of molecular conformation and chemical features arrangement. As a result, ROCS shows high success rate in the identification of molecules with novel cores for a given target.

We believed that the excellent activity of the resorcinol scaffold, in concert with new synthetic methodologies, would provide a good starting point for the synthesis of novel analogs, and as such, our Hsp90 drug discovery program was also based on the resorcinol class.

In this study, we selected the potent compound **AT-13387** with resorcinol core as the reference molecule for the construction of ROCS model. The model was validated by a decoy set download

from Directory of Useful Decoys (DUD, http://dud.docking.org/) containing 979 compounds with similar physicochemical properties to **AT-13387**. The model can accurately recognize the active compounds from the decoy set based on the molecular shape similarity. After validation, the model is applied to virtually screen the Topscience database (www.tsbiochem.com). The top 50 compounds by the scoring function of ROCS were purchased from Topscience for biological test. The inhibition effect of these 50 compounds against Hsp90 was firstly evaluated using Malachite Green assay. 11 compounds with over 60% inhibition rate at 40 μM were selected for reevaluation by the Discover RX ADP Hunter™ Plus Assay kit (ADP assay). Most of them showed moderate inhibition potency against Hsp90. Compound **36** containing the 5,6,7,8-tetrahydropyrido[4,3-d]pyrimidine core displayed the most potent inhibition (IC_{50} 45.39 ± 2.82 μM) in the fluorescence polarization (FP) assay. The binding mode of **36** with Hsp90 was predicted by molecular docking and guided by the revealed information, eight derivatives of **36** were designed and synthesized. These derivatives showed much improved potency both in target-based level and cell-based level. The most potent compound **57h**, exhibited over 450-fold improvement in Hsp90 inhibition (IC_{50} 0.10 ± 0.01 μM) and over 27-fold in antiproliferative effect in MCF cells (1.91 ± 1.21 μM) compared to **36**. Western blot analysis confirmed that **57h** downregulated a series of client proteins of Hsp90, including Her2, Erk, AKT and Raf-1 in a concentration-dependent manner. The induced Hsp70 expression, another hallmark of Hsp90 inhibition, was also observed. Our data prove the ligand-based method ROCS combined with structure-based modification can be well applied in the identification of novel Hsp90 inhibitors and more chemotypes are expected to be discovered by this method. Besides, compound **57h** can be used as an ideal lead for further optimization. The ligand-based method we reported here, was meaningful to guide the researchers to efficaciously identify novel inhibitors, especially for those targets with potent ligands.

2. Result and discussion

2.1. Generation and validation of ROCS model based on *AT-13387*

ROCS is a fast shape comparison application, based on the idea that molecules have similar shape if their volumes overlay well and any volume mismatch is a measure of dissimilarity. It uses a smooth Gaussian function to represent the molecular volume [43], so it is possible to routinely minimize to the best global match. A recent study suggested that the bioactive conformation of a reference molecule is not needed for the enrichment of shape based screening [44]. In this study, the promising Hsp90 inhibitor **AT-13387** was selected as the reference compound to generate the ROCS model. The molecular shape of **AT-13387** was depicted in gray shadow (Fig. 2A). The 3D similarity of a given compound to **AT-13387** was ranked by two methods: a) The molecular shape similarity and b) The combo score method, which was consisted of the shape Tanimoto coefficient and the score retrieved from the ROCS color force field. In this chemical force field, a molecule is described by the spatial arrangement of six types: hydrogen-bond donors, hydrogen-bond acceptors, hydrophobes, anions, cations, and rings. ROCS color force field can be used to measure chemical features complementarity, and to refine shape based superpositions based on chemical similarity. As both scores vary from 0 to 1, the combo score as the sum of both varies between 0 and 2 [45].

In order to validate the reliability of the model, an active set including 31 compounds was collected from literatures [34,46]. The decoy set including 979 compounds was downloaded from Hsp90 package in DUD. The multiple conformation of the active and decoy compounds were generated by OMEGA in Openeye. The validation was performed according to the shape similarity (Fig. 3A) and the combo score (Fig. 3B), respectively. Both the methods can well distinguish the active compounds from the decoy compounds. For shape similarity, most of the active compounds were above 0.6, while the decoy compound were lower than 0.6. For combo score, most of the active compounds were above 1.2, while about 80% of the compounds in decoy set were less than 1.0.

To avoid potential bias of the validation results due to large differences in molecular properties, we compared the basic physicochemical properties between active set and decoy set, the average values were shown in Table 1. The active set compounds have two HBA less than the decoy set compounds, meanwhile, the PSA of the active set is lower than the decoy set. However, the other key physicochemical properties such as molecular weight, HBD, rotatable bond and Log *D* are similar, indicating no potential bias exists in the validation of the overlays. As a result, we believe the overlays are reliable for the further virtual screening study.

2.2. Database screening for potential Hsp90 inhibitors

To identify novel Hsp90 inhibitors, the Topscience database (over 1.5 million compounds) was used to carry out the virtual screening using the ROCS model. The multiple conformations of

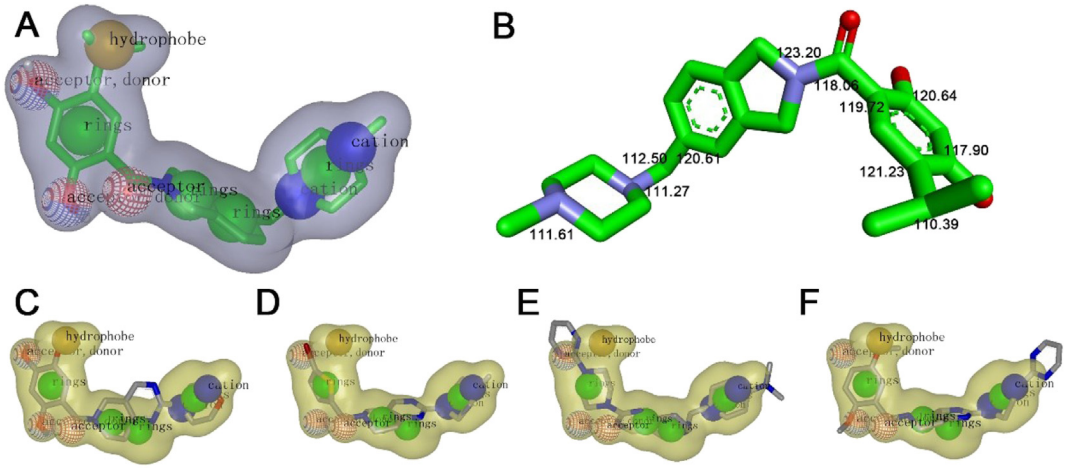

Fig. 2. (A) The ROCS model generated from **AT-13387**; (B) The bound conformation of **AT-13387** in the co-crystal structure (PDB id: 2XJX); (C) ~ (F) The overlay of the hit compounds **1**, **21**, **27** and **36** to the ROCS model, respectively.

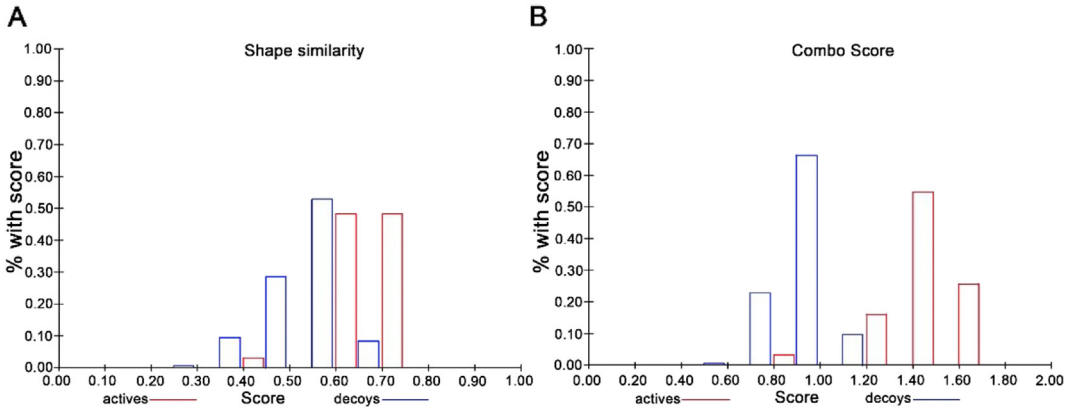

Fig. 3. The validation of the ROCS model based on **AT-13387**. An active set containing 31 compounds and a decoy set containing 979 compounds were applied for the validation. (A) The validation results based on shape similarity; (B) The validation results based on combo score.

different query molecules were calculated using OMEGA (default settings, with a maximum of 400 conformations per molecule). In the subsequently virtual screening, the query molecules were ranked by the shape similarity and the combo score. The top fifty compounds (in Supplementary data) were purchased from Topscience for further biological evaluation.

2.3. Biological assay of the hit compounds

To characterize the inhibition of Hsp90 by the 50 compounds, malachite green assay for inorganic phosphate was initially used to measure the ATPase activity of Hsp90. Malachite green assay was a colorimetric assay which was well suited to the automation required for high throughput screening as a rough and fast evaluation methodology [47,48]. 11 of 50 compounds (Fig. 4) showed over 60% inhibition rate at 40 μM (in Supplementary data).

We then analyzed the shape similarity and the combo score of these compounds (Table 2). For shape similarity, the values of the 11 compounds were ranging from 0.623 to 0.735. As shown in Fig. 3A, most of the compounds in the active set had the shape similarity over 0.6, therefore, these compounds were recognized as actives by ROCS model. Oppositely, for combo score, the values of the 11 compounds were ranging from 0.935 to 1.119, which was recognized as inactive in the model validation (Fig. 3B, most of the actives were over 1.2). This deviation can be explained by the very low chemical features similarity between the hits and the template molecules (Table 2). Considering these results, shape similarity evaluation can help us screen out more hits which might be omitted by combo score, thus might be more proper in the evaluation of the hits from virtual screening than combo score. In the chemical database containing huge compounds, a hit compound may have totally different spatial location and the arrangement of chemical features compared to the template molecule, but form a very similar molecular shape, thus has similar biological functions. Therefore, shape-based virtual screening is efficacious in the identification of novel hits.

Table 1
The comparison of the physicochemical properties of the active set, decoy set and the hits.

	MW[a]	HBA[b]	HBD[c]	RB[d]	PSA[e]	Log *D*
Active set	355.80	1.45	2.16	3.65	69.62	2.97
Decoy set	350.49	3.19	2.31	4.89	108.09	2.70
Hits	419.40	4	0.09	4.54	66.81	2.72

[a] Molecular weight.
[b] Hydrogen-bond acceptor.
[c] Hydrogen-bond donor.
[d] Rotatable bond.
[e] Polar surface area.

From the structures of the 11 compounds, it was striking to observe that they possessed the same core, tetrahydropyrido[4,3-d] pyrimidine. To confirm the results of malachite green assay, we performed another assay using Discover RX ADP Hunter™ Plus Assay kit. Most compounds except compound **7** showed consistent effects to the results of malachite green assay (Table 3). The most potent compound **36** exhibited a dose-dependent inhibitory manner with IC_{50} 35.18 ± 3.72 μM (Fig. 5A). Next, the four best compounds **13**, **14**, **27** and **36** in this round of assay were selected for further FP competitive binding assay to avoid false positives. Only compound **36** showed moderate inhibition activity (IC_{50} 45.39 ± 2.82 μM, Table 3).

To further confirm the Hsp90 inhibitory activities of **36**, we prepared a luciferase reporter assay by detecting the expression level of Hsp70, a key Hsp family member that was upregulated when Hsp90 was inhibited. As expected, **36** showed moderate Hsp70 induction in a dose-dependent manner, it showed over 1.5 times induction of Hsp70 at the concentration of 10.0 μM (Fig. 5B). The data further supported that **36** inhibited the activity of Hsp90 in a cell-based level. On the basis of these findings, compound **36** was selected for structural optimization with the aim to improve its activity in not only target-based but also cell-based level.

2.4. Design of new derivatives based on hit compound *36* and precursor evaluation

To analyze the binding mode of Hsp90 with **36**, it was docked in to active site of Hsp90 (PDB code: 2XJX). We could observe that 2,5-dimethoxy benzyl (fragment A) of **36** inserted into the bottom of the ATP-binding pocket comprised by the residues Asp93, Asn51 and Thr184, and 2-(1-piperazinyl)pyrimidine (fragment B) of **36** located at the edge of the pocket, pointing into the solvent accessible area (Fig. 6A and B). The general molecular orientation and the spatial location of the chemical features of **36** were similar to that of **AT-13387**. However, we found the location of 2,5-dimethoxy benzyl moiety was different from the resorcinol of **AT-13387**. We deduced the variation was caused by the flexibility of the carbon–nitrogen bond in compound **36**. In addition, we observed this bond was close to the hydroxyl group of Thr184, a key residue for the recognition of Hsp90. Therefore, the carbon–nitrogen bond was replaced by the carbonyl group. The resulted compound **57a** was docked into the active site (Fig. 6C and D). The binding mode of **57a** was in good agreement with our hypotheses: the introduced carbonyl formed a

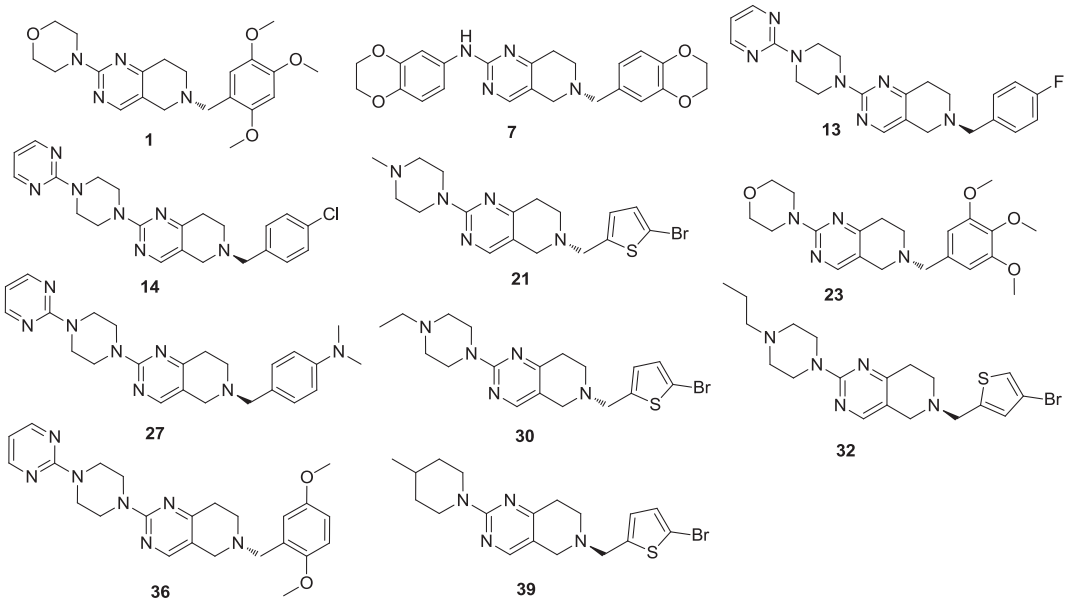

Fig. 4. The structures of 11 compounds over 60% inhibition rate in the Malachite Green Assay.

direct hydrogen bond with the side chain of Thr184. **57a** was subsequently synthesized (see Chemistry, Scheme 1) and showed slight improvement in affinity for Hsp90 in the FP and ADP assay, respectively (Table 4). Similar manner was also observed in compounds **57b** and **57c**, compared to their counterparts **13** and **14** without the carbonyl group. However, **57b** and **57c** displayed lower activity compared to **57a**, indicating methoxy substitution was more favorable than F or Cl. This phenomenon could be attributed to the H-bond recognition between methoxyl and Hsp90.

Further analysis of the binding mode of **57a** indicated that methoxyl at 5 position of 2,5-dimethoxy benzyl was too close to a sub-pocket formed by Leu107, Phe138, and Val150 (Fig. 6C and D). This can cause unfavorable intermolecular energy. Therefore, we next move the methoxyl group to the 4 position of 2,5-dimethoxy benzyl. The resulted compound **57d** show obviously improved activity compared to **57a** (Table 4). Binding mode analysis suggested that methoxyl group at R_2 position can facilitate an additional indirect hydrogen bond with the amine on Asn51 aided by the conserved water molecular W1 (Fig. 6E and F).

Further work on this study was focused on the enhancement of Hsp90 inhibitory and antiproliferative activity of **57d**. The binding mode of **57d** with Hsp90 suggested that 2- and 4-methoxy groups only interacted with the conversed water molecular W1 and W2, rather than directly interacted with two polar residues Asp93 and Asn51. As the two residues were recognized as the most significant points for Hsp90 to recognize the inhibitors through forming hydrogen bond networks with the conserved water molecules around the two residues [33], we therefore changed the dimethoxyphenyl ring into the resorcinol moiety. Encouragingly, the resulted compound **57e** (see Chemistry, Scheme 1), showed much better Hsp90 inhibitory activity than **57d** (Table 4). Binding mode of **57e** with Hsp90 showed direct hydrogen bonds between the hydroxyl of the resorcinol moiety with Asp93 and Asn51 and conversed water molecules (Fig. 7A and B).

However, this compound missed the occupation of the sub-pocket consist of Leu107, Phe138, and Val150, as a result, although the activity increased, it still belong to the micromolar range. With the aim to enhance the Hsp90 inhibitory activity to nanomolar range, we tried to occupy the sub-pocket by modifying the substituents on the resorcinol moiety. As we previously mentioned that the methoxyl was too large for the sub-pocket, we further designed compound **57f** with chloro substitution at 5 position of 2,5-dimethoxy benzyl (see Chemistry, Scheme 1). The FP assay showed that **57f** was much more potent than **57e**, with the low micromolar IC_{50} 1.67 ± 0.97 μM. The ADP assay also showed

Table 2
The shape similarity, chemical features similarity and combo score of the 11 hit compounds.

Compd. no.	Shape similarity	Chemical features similarity	Combo score
1	0.735	0.250	1.119
7	0.708	0.170	1.024
13	0.627	0.202	0.935
14	0.629	0.202	0.937
21	0.669	0.220	0.985
23	0.643	0.214	0.981
27	0.625	0.212	0.946
30	0.623	0.275	1.000
32	0.642	0.236	0.992
36	0.656	0.190	0.974
39	0.681	0.212	0.972

Table 3
Hsp90 ATPase activity inhibition (IC_{50}) in the ADP and FP assay by the 11 compounds over 60% inhibition in the Malachite Green Assay.

Compd. no.	Hsp90-ATPase activity inhibition (μM)[a]	Binding Hsp90 (FP, μM)[a]
1	50.90 ± 4.31	ND
7	>100	ND
13	40.24 ± 3.22	>100
14	47.88 ± 2.91	>100
21	63.20 ± 1.73	ND
23	55.12 ± 6.11	ND
27	46.13 ± 0.49	>100
30	74.68 ± 1.12	ND
32	59.28 ± 3.25	ND
36	35.18 ± 3.72	45.39 ± 2.82
39	87.96 ± 1.25	ND
17-DMAG	1.41 ± 0.05	0.09 ± 0.02
AT-13387	0.35 ± 0.11	0.03 ± 0.01

[a] Values shown are mean ± SD ($n = 3$).

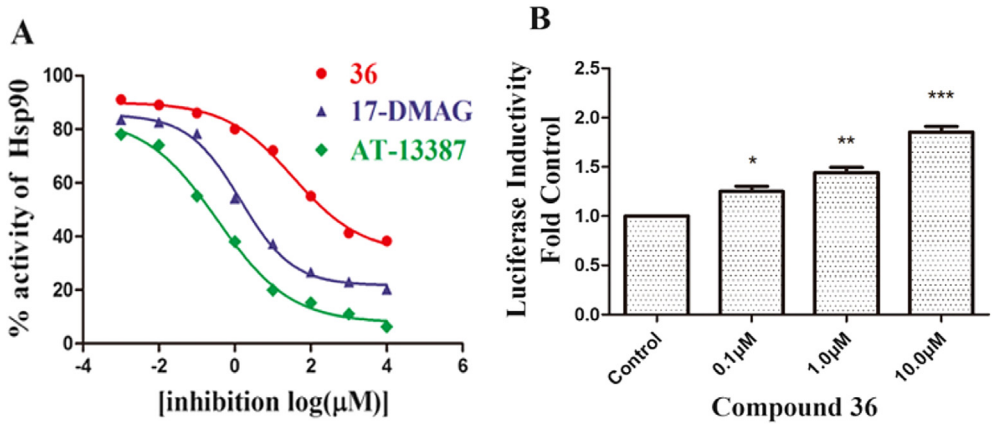

Fig. 5. The biological evaluation of the most potent compound **36**. (A) The dose-dependent inhibitory manner of **36** in the ADP assay. (B) The Hsp70 induction of Hsp70 in SK-Br-3 cell after the treatment of **36**.

similar manner, with a 4-fold improvement in IC_{50} values compared to **57e** (Table 4). The introduction of 5-chloro moiety also increased the antiproliferative potency in the four evaluated cell lines. The binding mode of **57f** with Hsp90 showed the 5-chloro moiety of **57f** pointed to the sub-pocket as expected (Fig. 7C and D). This is in good agreement with the observation of Roe et al. [49].

However, **57f** was still much less potent than the reference compound **AT-13387** and **17-DMAG**. To achieve the nanomolar goal, we further analyzed the scaffold of **57f**. As inspired by the docking, the 2-(piperazin-1-yl)pyrimidine moiety was not inserted into the ATP binding pocket of Hsp90, but pointed to the solvent area at the edge of the binding groove. As this area was not important for the

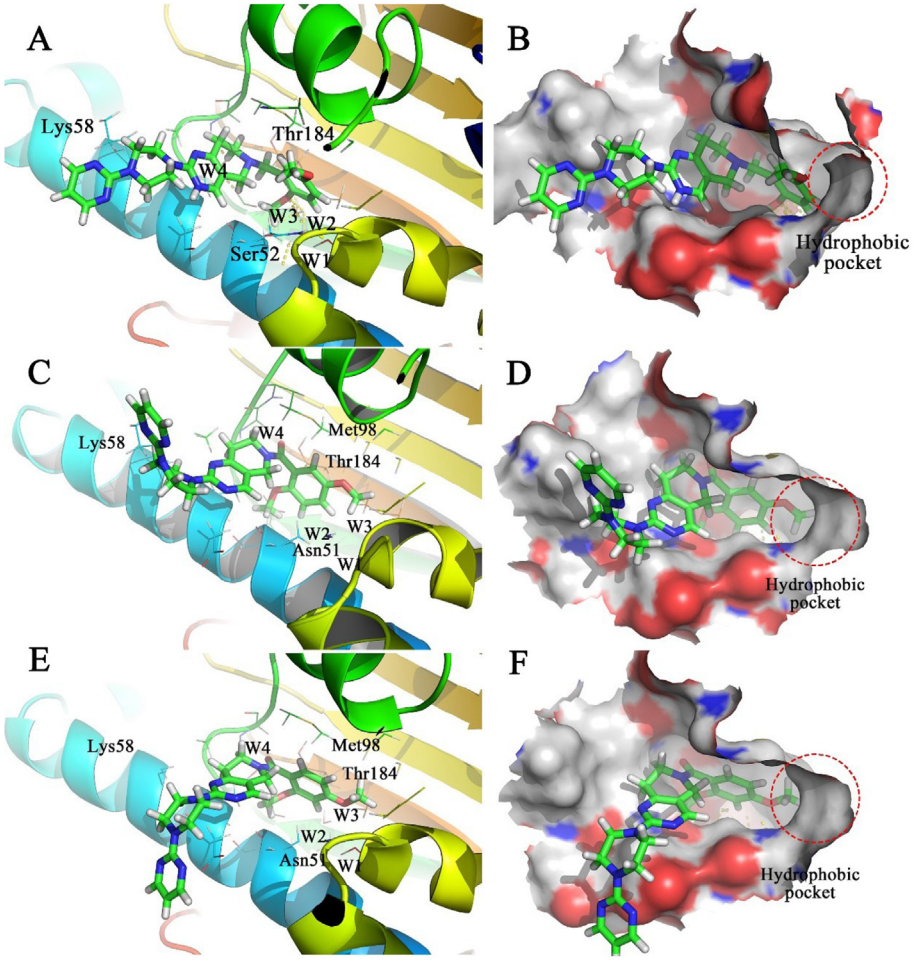

Fig. 6. The binding patterns of between the potent compounds and Hsp90. (A, C, E) **36**, **57a** and **57d** in the active site of Hsp90 respectively, key residues were labeled in stick; (B, D, F) **36**, **57a** and **57d** inserted into the active site of Hsp90 with a surface colored by electrostatic state.

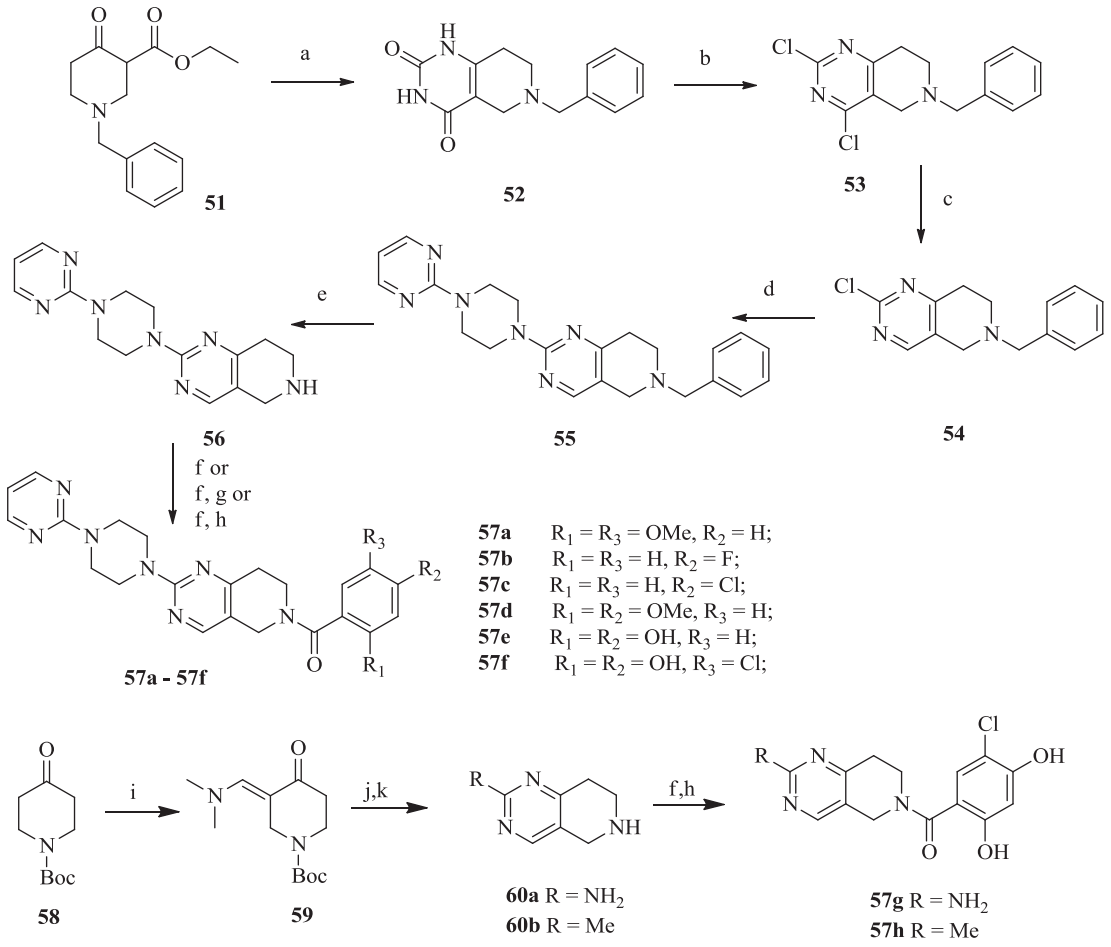

Scheme 1. Synthesis of compounds **57a**–**57h**. Reagents and conditions:(a) urea, MeONa, EtOH, reflux, 24 h, 75%; (b) $POCl_3$, N_2, 3 h, 87%; (c) activated Zn, NH_4OH, EtOH, reflux, 12 h, 61%; (d) 1-(2-Primidinyl)piperazine, Na_2CO_3, dioxane, 85 °C, 6 h, 75%; (e) 10% Pd/C, H_2, MeOH, rt, 15 h, 81%; (f) substituted benzoic acid, EDCI, HOBt, Et_3N, dichloromethane, rt, 12 h, 88%; (g) 10% Pd/C, H_2, MeOH, rt, 2 h, 80%; (h) BBr_3, dichloromethane, 0 °C, 3 h, 45%; (i) N,N-dimethylformamide dimethyl acetal, reflux, 1.5 h; 79%; (j) guanidine carbonate or acetamidine hydrochloride, sodium acetate, EtOH, reflux, 42 h, 83%; (k) TFA, 0 °C, 1 h, 95%.

recognition of Hsp90 inhibitors, the extra solvation energy of this moiety was unfavorable for the binding affinity. Besides, the molecular weight of **57f** was 467, which was too high for an ideal lead compounds for further optimization. The high molecular weight also lead to low ligand efficiency, which was recognized as a critical profile for a drug candidate. Taken these facts into consideration, we next removed the 2-(piperazin-1-yl)pyrimidine (fragment B) to obtain compound **57g** and **57h** (see Chemistry, Scheme 1). To our delight, the two compounds exhibited much higher potency compared to **57f** in both target-based and cell-based level. Compound **57g** exhibited nanomolar activity in Hsp90 assay (IC_{50} 0.31 ± 0.13 μM and 0.51 ± 0.21 μM in FP assay and ADP assay, respectively, Table 4), meanwhile, compound **57h** exhibited comparable activity to the positive control **17-DMAG** and **AT-13387**, in not only Hsp90 assay (IC_{50} 0.10 ± 0.01 μM and 0.42 ± 0.11 μM in FP assay and ADP assay, respectively, Table 4) but also antiproliferative assay of the four cell lines. **57h** with a methyl substituted the fragment B, showed the best activity. This indicated that

Table 4
Antiproliferative activity in several cell lines, Hsp90 ATPase activity inhibition in the ADP and FP assay by the compounds **57a**–**57h**.

Compd. no.	Antiproliferative activity cell lines (IC_{50}, μM)[a]				Hsp90-ATPase activity inhibition (IC_{50}, μM)[a]	Binding Hsp90 (FP, IC_{50}, μM)[a]
	SK-Br-3	MCF-7	HCT116	A231		
36	10.73 ± 1.21	53.25 ± 3.13	43.20 ± 1.45	27.53 ± 2.71	35.18 ± 1.75	45.39 ± 2.83
57a	23.54 ± 1.42	43.31 ± 1.91	34.56 ± 1.02	51.32 ± 1.93	16.44 ± 1.51	40.36 ± 0.34
57b	24.5 ± 1.30	46.17 ± 4.54	67.89 ± 2.75	54.44 ± 1.61	27.21 ± 2.17	>100
57c	11.23 ± 1.71	42.16 ± 3.75	21.68 ± 6.20	24.60 ± 4.11	24.48 ± 1.92	>100
57d	16.01 ± 1.63	20.16 ± 2.84	11.48 ± 1.44	37.60 ± 3.26	7.88 ± 0.93	30.54 ± 1.68
57e	12.23 ± 1.81	17.52 ± 0.34	23.14 ± 2.82	21.32 ± 1.11	3.23 ± 0.62	10.23 ± 2.55
57f	5.17 ± 0.43	10.22 ± 1.25	2.74 ± 1.57	6.65 ± 0.39	0.93 ± 0.21	1.67 ± 0.97
57g	2.30 ± 0.11	4.41 ± 1.03	1.21 ± 0.23	5.22 ± 1.08	0.51 ± 0.21	0.31 ± 0.13
57h	4.32 ± 0.74	1.91 ± 1.21	2.82 ± 0.92	3.76 ± 0.56	0.42 ± 0.11	0.10 ± 0.01
17-DMAG	3.11 ± 0.21	0.8 ± 0.32	1.21 ± 0.21	0.17 ± 0.07	1.41 ± 0.05	0.09 ± 0.02
AT-13387	0.14 ± 0.01	0.28 ± 0.07	0.08 ± 0.02	1.01 ± 0.42	0.34 ± 0.11	0.03 ± 0.01

[a] Values shown are mean ± SD ($n = 3$).

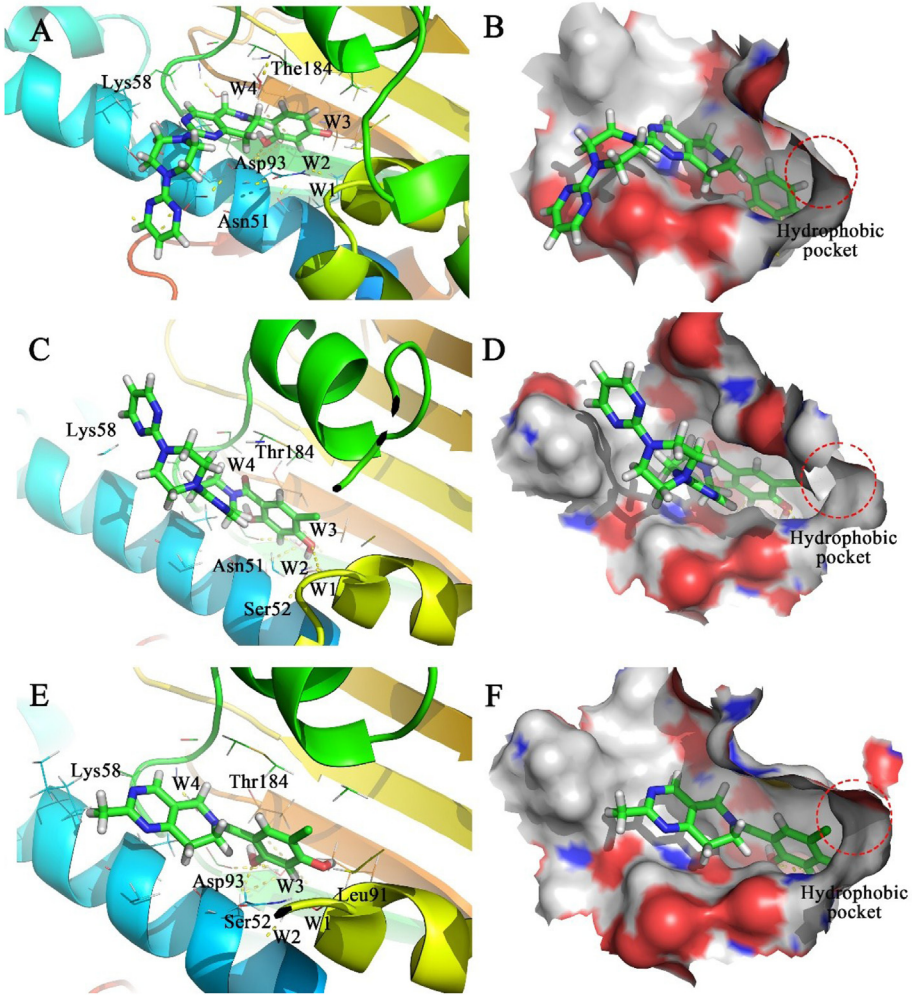

Fig. 7. The binding patterns of between the potent compounds and Hsp90. (A, C, E) **57e**, **57f** and **57h** in the active site of Hsp90 respectively, key residues were labeled in stick; (B, D, F) **57e**, **57f** and **57h** inserted into the active site of Hsp90 with a surface colored by electrostatic state.

hydrophobic side chains at this position were preferable to the polar groups. Compared to **AT-13387**, the novel tetrahydropyrido [4,3-d]pyrimidines core of **57h** may stabilize the molecule in the binding groove by the extra polar contacts through the N atoms in the ring (Fig. 7E and F).

Subsequently, we conducted a luciferase reporter assay by detecting the expression level of Hsp70. **57h** showed the obvious Hsp70 induction in a dose-dependent manner, it showed over 3 times induction of Hsp70 at the concentration of 1 μM (Fig. 8A). Encouraged by these results, the ability of **57h** to affect turnover of several Hsp90 client proteins in SK-Br-3 cells was also assessed. As shown in Fig. 8B, **57h** dose-dependently induced the degradation of Hsp90 client proteins Her2, Akt, Erk and Raf-1, which was in a similar manner with that in the anti-proliferative assay. At the same

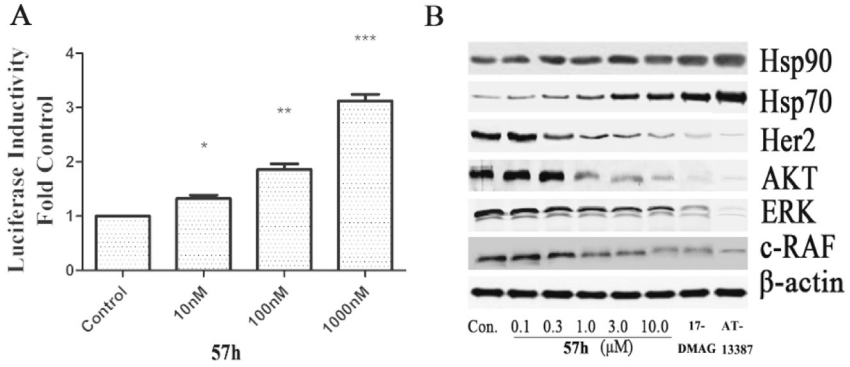

Fig. 8. The biological evaluation of the most potent compound **57h**. (A) The Hsp70 induction of Hsp70 in SK-Br-3 cell after the treatment of **57h**. (B) Western-Blot analysis of the expression level of Hsp90, Hsp70 and several client proteins of Hsp90 after incubation with **57h** in SK-Br-3 cells. **17-DMAG** and **AT-13387** were used as positive control at 1.0 μM. **57h** was incubated with SK-Br-3 cancer cells at indicated concentrations (μM) for 36 h. Cell extracts were prepared and equivalent amounts of protein were separated by SDS-PAGE and subsequently western-blotted for the indicated proteins.

time, **57h** dose-dependently up-regulated Hsp70. All the data confirmed **57h** as potent Hsp90 inhibitor.

2.5. Chemistry

The synthesis routes used to prepare compounds **57a**–**57h** were depicted in Scheme 1. Compounds **57a**–**57f** were prepared in an analogous manner starting from the commercially available ethyl 1-benzyl-4-oxopiperidine-3-carboxylate (compound **51**, Scheme 1). **52** was prepared by amination of **51** with urea under basic conditions. Then, **52** was treated with $POCl_3$ to provide the desired intermediate **53**. **53** was reduced by Zn to give compound **54**. The intermediate **55** was obtained by reaction of **53** and commercially available 1-(2-Pyrimidinyl)piperazine. The benzyl group of **55** was removed by Pd/C to afford the key intermediate **56**. Finally, **57a**–**57f** were obtained by coupling the key intermediate **56** with the appropriate substituted benzoic acid using standard EDCI/HOBt coupling conditions. Compounds **57g** and **57h** were prepared in an analogous manner starting from the commercially available compound **58**. Reaction of the compound **58** with N,N-dimethylformamide dimethyl acetal at reflux afforded **59**. The intermediate **59** was treated by guanidine carbonate or acetamidine hydrochloride in ethyl alcohol in the presence of sodium acetate to provide intermediates **60a** and **60b**. Compounds **57g** and **57h** were obtained from **60a** and **60b** in the same way as **57a** - **57f**.

3. Conclusion

In this study, a ROCS model on the basis of **AT-13387** was established and validated to screen Topscience database, from which 11 compounds containing the similar scaffold were identified as potent inhibitors of molecular chaperone Hsp90. Among all of the 11 compounds, compound **36** demonstrated the most potent inhibitory activity (IC_{50} of 35.18 ± 3.72 μM, 45.39 ± 2.82 μM for ADP and FP assay, respectively). Anti-proliferative assay results also showed that compound **36** had the potential to be developed as an anti-proliferative agent against cancer cells. To improve potency of the hit **36**, we designed and synthesized eight analogs aided by structure-based design using docking simulation. As we expected, most derivatives showed improvement potency both in target-based and cell-based assay, and the most potent derivative **57h** showed over 450-fold improvement in Hsp90 inhibition compared to the original hit **36**, with IC_{50} 0.42 ± 0.11 μM and 0.10 ± 0.01 μM in the ADP and FP assay respectively. In addition, **57h** displayed much better potency in affecting the degradation of client proteins and cell proliferation in Sk-Br-3 cell. These results provided important information for further structural modifications of **57h** to develop novel potent Hsp90 inhibitors.

By analyzing the biological data, we summarize the SAR as follows (Fig. 9): i) the fragment A inserted into the active site comprised by the residues Asp93, Asn51 and Thr184, and the fragment B made no direct contact with the protein and was directed towards solvent; ii) the introduction of the carbonyl, 2-OH and 4-OH improved the potency by formed H-bond with the residues Thr184, Asp93 and Asn51; iii) the chloro at 5-position was important for cytotoxicity; iv) the fragment B could be replaced by the amino or methyl group, and the methyl group in this position was favorable for the Hsp90 inhibition activities.

The ligand-based method we reported here, was also efficacious and meaningful to guide the researchers to identify novel inhibitors, especially for those targets with potent ligands.

4. Experimental

4.1. Chemistry

Melting points were determined on a Mel-TEMP II melting point apparatus and are uncorrected. ^{1}H NMR spectra were recorded with

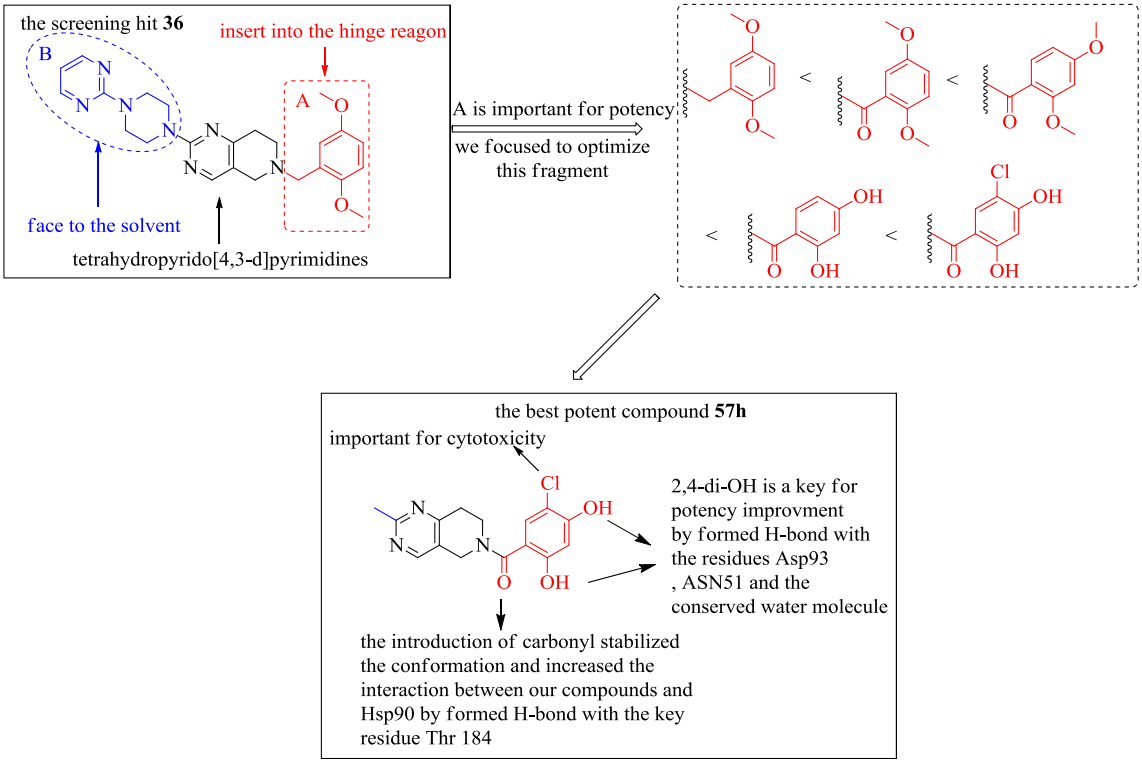

Fig. 9. Structure–activity relationships of the optimized compounds based on the screening hit **36**.

a Bruker Avance 300 MHz spectrometer at 300 K, using TMS as an internal standard. MS spectra were recorded on a Shimadzu GC–MS 2010 (EI) or a Mariner Mass Spectrum (ESI), or a LC/MSD TOF HR-MS Spectrum. All compounds were routinely checked by TLC and ^{1}H NMR. TLCs and preparative thin-layer chromatography were performed on silica gel GF/UV 254 supported by glass plate, and the chromatograms were performed on silica gel (200–300 mesh) visualized under UV light at 254 and 365 nm. Purity for final compounds was greater than 95% and was measured by HPLC with Agilent Technologies 1260 infinity C18 4.60 mm × 150 mm column using a mixture of solvent methanol/water at the flow rate of 0.5 mL/min and peak detection at 245 nm under UV. All solvents were reagent grade and, when necessary, were purified and dried by standards methods. Concentration of solutions after reactions and extractions involved the use of a rotary evaporator operating at a reduced pressure of ca. 20 Torr. Organic solutions were dried over anhydrous sodium sulfate. Analytical results are within (0.40% of the theoretical values).

4.1.1. 6-Benzyl-5,6,7,8-tetrahydropyrido[4,3-d]pyrimidine-2,4(1H,3H)-dione **52**

A commercially available compound **51** (10.0 g, 33.5 mmol) was dissolved in ethanol (150.0 mL), then urea (10.0 g, 167.0 mmol) and sodium methoxide (22.7 g, 118.0 mmol) were added thereto and the mixture was made to react for 24 h under the condition of heating to reflux. After cooled to 0 °C, crystals separated out therefrom were filtered. The crystals were suspended in water, hydrochloric acid (6.0 mol/L) was added thereto and pH was adjusted to 6.0. Stirring was further conducted at room temperature for 1 h and the crystals separated out therefrom were filtered and dried *in vacuo* to prepare compound **52** (6.5 g, 75%), which was used without further purification. $R_f = 0.1$ (EA:MeOH = 5:1); Mp: 293 °C; ^{1}H NMR (300 MHz, $CDCl_3$, δ ppm): 2.43–2.45 (m, 2H), 2.51–2.52 (m, 2H), 3.01 (s, 2H), 3.53 (s, 2H), 7.23–7.41 (m, 5H), 10.21 (s, 1H), 11.01 (s, 1H).

4.1.2. 6-Benzyl-2,4-dichloro-5,6,7,8-tetrahydropyrido[4,3-d]pyrimidine **53**

52 (8.5 g, 32.9 mmol) was added to phosphoryl chloride (50.0 mL, 535 mmol) in a 250 mL round-bottom flask equipped with a stir bar, and the solution was refluxed for 3 h under N_2. The volatiles were removed under reduced pressure, and the concentrate was poured over 200 mL of ice. NaOH (3 M) was added to a final pH of 10, and then the aqueous phase was extracted with CH_2Cl_2 (3 × 100 mL). The combined organics were dried over $MgSO_4$, filtered, and concentrated to a tan oil. This crude material was dissolved in dichloromethane, concentrated onto silica gel, and subjected to column chromatography using a 100 g column, with a gradient of 0%–50% ethyl acetate in hexanes. The product-containing fractions were combined and evaporated under reduced pressure to give **53** as a pale solid (8.4 g, 87%). $R_f = 0.5$ (PE:EA = 8:1); Mp: 273–275 °C; ^{1}H NMR (300 MHz, $CDCl_3$, δ ppm): 2.23–2.24 (m, 2H), 2.41–2.43 (m, 2H), 2.97 (s, 2H), 3.53 (s, 2H), 7.53–7.61 (m, 5H).

4.1.3. 6-Benzyl-2-chloro-5,6,7,8-tetrahydropyrido[4,3-d]pyrimidine **54**

To a solution of **53** (8.0 g, 27.3 mmol) in ethanol (150.0 mL) was added zinc (14.2 g, 218.4 mmol) and ammonium hydroxide (18.9 mL, 136.5 mmol) and the reaction was heated to 78 °C for 15 h. The reaction was cooled, filtered through Celite, and washed with ethyl acetate. The reaction was extracted with ethyl acetate (3 × 200 mL) and the organic phase was dried over $MgSO_4$. The organic phase was concentrated and purified by normal phase column chromatography (0–100% ethyl acetate in hexanes) to afford 4.3 g (61%) of **54** as a white solid. $R_f = 0.2$ (PE:EA = 8:1); Mp: 253–254 °C; ^{1}H NMR (300 MHz, $CDCl_3$, δ ppm): 2.33–2.35 (m, 2H), 2.52–2.53 (m, 2H), 3.11 (s, 2H), 3.53 (s, 2H), 7.13–7.39 (m, 5H), 8.53 (s, 1H).

4.1.4. 6-Benzyl-2-(4-(pyrimidin-2-yl)piperazin-1-yl)-5,6,7,8-tetrahydropyrido[4,3-d]pyrimidine **55**

54 (4.0 g, 15.4 mmol) was dissolved in dioxane (100.0 mL), then 1-(2-Pyrimidinyl)piperazine (5.1 g, 30.8 mmol) and sodium carbonate (16.3 g, 154.0 mmol) were added thereto and the mixture was stirred at 90 °C for 30 h. The resulting reaction was filtered to remove sodium carbonate, extraction was conducted by addition of water and chloroform to the filtrate and the organic layer was dried over magnesium sulfate. After evaporation of the solvent, a mixed solvent of hexane/ethyl acetate (5:1) was added and the suspension was stirred for 1 h. After that, the crystals separated out therefrom were filtered and dried *in vacuo* to prepare compound **55** (4.5 g, 75%). $R_f = 0.4$ (PE:EA = 1:2); Mp: 179–181 °C; ^{1}H NMR (300 MHz, $CDCl_3$, δ ppm): 2.43–2.45 (m, 2H), 2.82–2.83 (m, 2H), 3.51 (s, 2H), 3.63 (s, 2H), 3.82 (s, 8H), 6.51–6.54 (m, H), 7.27–7.41 (m, 5H), 8.00 (s, 1H), 8.34–8.36 (s, 2H). MS (Mwt.: 387.48): *m*/*z* 387 (M+, 100%), 372 (8%), 253 (80%), 134 (95%).

4.1.5. 2-(4-(Pyrimidin-2-yl)piperazin-1-yl)-5,6,7,8-tetrahydropyrido[4,3-d]pyrimidine **56**

55 (4.3 g, 11.1 mmol) was dissolved in MeOH (18.0 mL) and dichloromethane (5 mL), treated with 10% Pd/C (50.0 mg), then subjected to hydrogenation at atmospheric pressure for 16 h. The mixture was filtered through Celite and washed with MeOH. The combined filtrates were concentrated *in vacuo*. The residue was triturated with Et_2O, filtered, and then dried under vacuum to give the title compound as an off-white solid (2.64 g, 80%). Mp: 163 °C; ^{1}H NMR (300 MHz, $CDCl_3$, δ ppm): 2.51–2.52 (m, 2H), 2.70–2.72 (m, 2H), 3.01–3.04 (m, 2H), 3.61–3.82 (m, 8H), 6.64–6.67 (m, 1H), 8.10 (s, 1H), 8.40 (d, $J = 4.74$, 2H). MS (Mwt.: 297.36): *m*/*z* 297 (M+, 15%), 163 (73%), 134 (100%).

4.1.6. (2,5-Dimethoxyphenyl)(2-(4-(pyrimidin-2-yl)piperazin-1-yl)-7,8 dihydropyrido[4,3-d]pyrimidin-6(5H)-yl)methanone **57a**

A mixture of 2,5-dimethoxybenzoic acid (151.0 mg, 0.83 mmol), EDCI (192.0 mg, 1.0 mmol), HOBt (135.0 mg, 1.0 mmol) and **56** (300.0 mg, 1.0 mmol) in CH_2Cl_2 (10.0 mL) was stirred at room temperature overnight. The organic layer was washed successively with 2 M HCl and 2 M NaOH, then dried ($MgSO_4$), filtered, concentrated and purified by normal phase column chromatography (0–100% ethyl acetate in hexanes) to afford 336.0 mg (88%) of **57a** as a white solid. $R_f = 0.2$ (PE:EA = 1:1); Mp: 189–191 °C; ^{1}H NMR (300 MHz, $CDCl_3$, δ ppm): 2.86 (s, 4H), 3.57 (s, 2H), 3.81 (s, 6H), 3.82–3.92 (m, 8H), 6.51–6.54 (m, 1H), 6.80–6.87 (m, 2H), 7.06 (s, 1H), 8.02 (s, 1H), 8.34–8.36 (m, 2H). ^{13}C NMR (75 MHz, $CDCl_3$, δ ppm): 169.11, 165.05, 158.32 (2C), 155.15, 154.95, 149.12, 125.83, 123.52, 121.51, 116.15, 114.10, 111.34, 56.21, 56.23, 46.01 (4C), 44.41, 43.22, 35.64. IR (KBr):3342, 3125, 2954, 1629, 1543, 1399, 1319, 1282, 1246, 1178, 971, 875, 732 cm^{-1}. HRMS (ESI): calcd for $C_{24}H_{27}N_7O_3$ $[M + H]^+$ 462.2175, found 462.2151. Purity: 98.83% by HPLC ($MeOH/H_2O$ = 80:20).

4.1.7. (4-Fluorophenyl)(2-(4-(pyrimidin-2-yl)piperazin-1-yl)-7,8-dihydropyrido[4,3-d]pyrimidin-6(5H)-yl)methanone **57b**

Compound **57b** (302.0 mg, 87% yield) was synthesized from 4-fluorobenzoic acid (116 mg, 0.83 mmol) and **56** (300.0 mg, 1.0 mmol) according to the procedure used to synthesize **57a**; $R_f = 0.4$ (PE:EA = 1:1); Mp: 196–198 °C; ^{1}H NMR (300 MHz, $CDCl_3$, δ ppm): 2.87 (s, 2H), 3.71 (s, 2H), 3.92 (s, 8H), 4.61 (s, 2H), 6.53–6.56

(m, 1H), 7.11–7.17 (m, 2H), 7.45–7.50 (m, 2H), 7.06 (s, 1H), 8.22 (s, 1H), 8.34–8.35 (m, 2H). ^{13}C NMR (75 MHz, $CDCl_3$, δ ppm): 171.03, 169.21, 164.90, 162.10, 161.98, 158.10 (2C), 155.23, 135.69, 131.26, 131.01, 124.01, 116.27, 115.78, 110.97, 45.98 (4C), 44.11, 43.55, 34.92. IR (KBr): 3404, 2957, 2862, 1629, 1581, 1466, 1348, 1252, 1047, 922, 863, 793, 719 cm^{-1}. HRMS (ESI): calcd for $C_{22}H_{22}FN_7O$ $[M + H]^+$ 420.1870, found 420.1873. Purity: 98.74% by HPLC (MeOH/H_2O = 80:20).

4.1.8. (4-Chlorophenyl)(2-(4-(pyrimidin-2-yl)piperazin-1-yl)-7,8-dihydropyrido[4,3-d]pyrimidin-6(5H)-yl)methanone ***57c***

Compound **57c** (307.0 mg, 85% yield) was synthesized from 4-chlorobenzoic acid (129 mg, 0.83 mmol) and **56** (300.0 mg, 1.0 mmol) according to the procedure used to synthesize **57a**; R_f = 0.4 (PE:EA = 1:1); Mp: 219–222 °C; ^{1}H NMR (300 MHz, $CDCl_3$, δ ppm): 2.86 (s, 2H), 3.65 (s, 2H), 3.92 (s, 8H), 4.51–4.71 (m, 2H), 6.53–6.56 (m, 1H), 7.27–7.46 (m, 4H), 8.00–8.25 (m, 1H), 8.34–8.37 (m, 2H). ^{13}C NMR (75 MHz, $CDCl_3$, δ ppm): 169.13, 163.15, 161.24, 161.02, 156.35 (2C), 153.98, 138.17, 136.95, 130.05 (2C), 127.83 (2C), 123.79, 110.23, 46.01 (4C), 44.34, 43.67, 35.02. IR (KBr): 2998, 2909, 2843, 1629, 1586, 1506, 1422, 1351, 1256, 1178, 1048, 978, 845, 759 cm^{-1}. HRMS (ESI): calcd for $C_{22}H_{22}ClN_7O$ $[M + H]^+$ 436.1574, found 436.1580. Purity: 99.30% by HPLC (MeOH/H_2O = 80:20).

4.1.9. (2,4-Dimethoxyphenyl)(2-(4-(pyrimidin-2-yl)piperazin-1-yl)-7,8-dihydropyrido[4,3-d]pyrimidin-6(5H)-yl)methanone ***57d***

Compound **57d** (333.0 mg, 87% yield) was synthesized from 4-chlorobenzoic acid (151.0 mg, 0.83 mmol) and **71** (300.0 mg, 1.0 mmol) according to the procedure used to synthesize **57a**; R_f = 0.2 (PE:EA = 1:1); Mp: 226–228 °C; ^{1}H NMR (300 MHz, $CDCl_3$, δ ppm): 2.72–2.88 (m, 2H), 3.51–3.56 (m, 2H), 3.80 (s, 6H), 3.82–3.89 (m, 8H), 4.51–4.78 (m, 2H), 6.45–6.52 (m, 3H), 7.18–7.26 (m, 1H), 8.12 (s, 1H), 8.29–8.34 (m, 2H). ^{13}C NMR (75 MHz, $CDCl_3$, δ ppm): 170.13, 165.33, 164.86, 162.02, 161.89, 161.17, 158.12 (2C), 154.01, 127.93, 125.98, 121.01, 109.83, 105.05, 98.54, 56.03, 57.98, 45.88 (4C), 43.65, 42.12, 33.98. IR (KBr):3430, 2906, 1630, 1586, 1507, 1419, 1258, 1084, 978, 839, 796, 757 cm^{-1}. HRMS (ESI): calcd for $C_{24}H_{27}N_7O_3$ $[M + H]^+$ 462.2175, found 462.2179. Purity: 99.23% by HPLC (MeOH/H_2O = 80:20).

4.1.10. (2,4-Dihydroxyphenyl)(2-(4-(pyrimidin-2-yl)piperazin-1-yl)-7,8-dihydropyrido[4,3-d]pyrimidin-6(5H)-yl)methanone ***57e***

Compound **57e** with benzyl protection(425.0 mg, 83% yield) was synthesized from 2,4-bis(benzyloxy)benzoic acid [add 3] (277.0 mg, 0.83 mmol) and **56** (300.0 mg, 1.0 mmol) according to the procedure used to synthesize **57a**; the product (400.0 mg, 0.65 mmol) was dissolved in MeOH (8.0 mL) and CH_2Cl_2 (3.0 mL), treated with 10% Pd/C (30.0 mg) then subjected to hydrogenation at atmospheric pressure for 2 h. The mixture was filtered through Celite and washed with MeOH. The combined filtrates were concentrated *in vacuo*. The residue was triturated with Et_2O, filtered and then dried under vacuum to give the title compound as an off-white solid (225.0 mg, 80%); R_f = 0.35 (EA:MeOH = 5:1); Mp: 290–291 °C; ^{1}H NMR (300 MHz, DMSO, δ ppm): 2.71–2.75 (m, 2H), 3.67 (s, 2H), 3.79 (s, 8H), 4.50 (s, 2H), 6.25–6.32 (m, 2H), 6.64–6.67 (m, 1H), 6.98 (d, J = 8.1, 1H), 8.24 (s, 1H), 8.38 (d, J = 4.5, 1H), 9.59 (s, 1H), 9.74 (s, 1H). ^{13}C NMR (75 MHz, DMSO, δ ppm): 169.18, 164.72, 161.40, 161.19, 160.29, 157.18 (2C), 155.29, 154.24, 128.80, 117.76, 114.32, 109.54, 104.51, 98.09, 43.08 (4C), 38.72, 32.05, 31.16. IR (KBr):3431, 3156, 2993, 2866, 1626, 1599, 1486, 1436, 1347, 1251, 1166, 1032, 975, 835, 789 cm^{-1}. HRMS (ESI): calcd for $C_{22}H_{23}N_7O_3$ $[M + H]^+$ 434.1862, found 434.1872. Purity: 98.46% by HPLC (MeOH/H_2O = 80:20).

4.1.11. (5-Chloro-2,4-dihydroxyphenyl)(2-(4-(pyrimidin-2-yl) piperazin-1-yl)-7,8-dihydropyrido[4,3-d]pyrimidin-6(5H)-yl) methanone ***57f***

Compound **57f** with benzyl protection (451.0 mg, 84% yield) was synthesized from 2,4-bis(benzyloxy)-5-chlorobenzoic acid (305.0 mg, 0.83 mmol) and **56** (300.0 mg, 1.0 mmol) according to the procedure used to synthesize **57a**; A stirred solution of the product (400.0 mg, 0.62 mmol) in CH_2Cl_2 (10.0 mL) at 0 °C was treated dropwisely with BBr_3 in CH_2Cl_2 (1.86 mL, 1 M) and the mixture was stirred for 3 h. The reaction was quenched by the addition of water then extracted with EtOAc. The organic phase was dried ($MgSO_4$), filtered and the solvent evaporated *in vacuo*. The crude material was purified by normal phase column chromatography (10% MeOH in EtOAc) to afford 130.0 mg (45%) of **57f** as a white solid. R_f = 0.4 (EA:MeOH = 5:1); Mp: 296 °C; ^{1}H NMR (300 MHz, DMSO, δ ppm): 2.73–2.76 (m, 2H), 3.71 (s, 2H), 3.80 (s, 8H), 4.52 (s, 2H), 6.35–6.37 (m, 1H), 6.65–6.68 (m, 1H), 7.11 (d, J = 8.1, 1H), 8.14 (s, 1H), 8.41 (d, J = 5.1, 1H), 9.63 (s, 1H), 9.94 (s, 1H). ^{13}C NMR (75 MHz, DMSO, δ ppm): 171.01, 164.52, 162.23, 162.01, 157.87 (2C), 156.81, 156.34, 153.25, 131.41, 124.61, 116.94, 113.56, 110.20, 103.01, 45.91, 43.74, 42.50, 34.13. IR (KBr):3432, 2853, 1629, 1600, 1584, 1500, 1436, 1347, 1253, 1187, 1059, 979, 735 cm^{-1}. HRMS (ESI): calcd for $C_{22}H_{23}ClN_7O_3$ $[M + H]^+$ 468.1473, found 468.1450. Purity: 98.71% by HPLC (MeOH/H_2O = 80:20).

4.1.12. (2-Amino-7,8-dihydropyrido[4,3-d]pyrimidin-6(5H)-yl)(5-chloro-2,4-dihydroxyphenyl)methanone ***57g***

N-tert-butoxycarbonyl-4-piperidone (**58**, 5.8 g, 31.4 mmol) was dissolved in N,N-dimethylformamide dimethyl acetal (45.0 mL), and the solution was heated under reflux for 1.5 h and concentrated. The residue was triturated with hexane, filtered, and washed with hexane to give **59** as a yellow powder (5.1 g, 63.8%): mp 135–136 °C; To a solution of **59** (5.0 g, 20.8 mmol) in EtOH (200.0 mL) were added guanidine carbonate (15.0 g, 84.0 mmol) and sodium acetate (13.7 g, 167.0 mmol), and the solution was heated under reflux for 48 h. The reaction mixture was filtered, and the insoluble material was extracted with $CHCl_3$ and washed with water. The organic layer was dried over anhydrous $MgSO_4$ and evaporated. The resultant solid was triturated with 2-propanol, filtered, and washed with 2-propanol and Et_2O to give a colorless powder. It was dissolved in TFA (50.0 mL) at 0 °C, and the solution was stirred at room temperature for 1 h and concentrated. The residue was dissolved in 2-propanol and treated with concentrated HCl (4.0 mL). The precipitated solid was filtered and washed with 2-propanol and Et_2O to give **60a** (4.2 g, 81.6%) as a colorless powder: Mp 258–260 °C; Compound **57g** was obtained from **60a** in the same way as **57f**. A white powder: yield 0.73 g (43%); R_f = 0.3 (EA:MeOH = 5:1); Mp: 281–282 °C; ^{1}H NMR (300 MHz, DMSO, δ ppm): 2.83–2.87 (m, 2H), 3.75–3.77 (m, 2H), 4.58–4.60 (m, 2H), 6.37 (s, 1H), 6.81–6.83 (m, 2H), 7.34 (s, 1H), 8.49 (s, 1H), 9.69–9.71 (d, 2H). ^{13}C NMR (75 MHz, DMSO, δ ppm): 171.42, 163.17, 161.02, 157.16, 156.32, 153.66, 133.72, 118.01, 117.54, 113.26, 102.18, 43.44, 42.54, 33.15. IR (KBr): 3152, 2360, 1609, 1565, 1477, 1258, 1198, 1049, 948, 839, 769 cm^{-1}. HRMS (ESI): calcd for $C_{14}H_{13}ClN_4O_3$ $[M + H]^+$ 321.0676, found 321.0685. Purity: 98.01% by HPLC (MeOH/H_2O = 80:20).

4.1.13. (2-Methyl-7,8-dihydropyrido[4,3-d]pyrimidin-6(5H)-yl)(5-chloro-2,4-dihydroxyphenyl)methanone ***57h***

Compound **57h** was obtained from **60b** in the same way as **57g**. A white powder: yield 0.84 g (51%); R_f = 0.3 (EA:MeOH = 10:1); Mp: 284–285 °C; ^{1}H NMR (300 MHz, DMSO, δ ppm): 2.53 (s, 3H), 2.81–2.85 (m, 2H), 3.66–3.69 (m, 2H), 4.61 (s, 2H), 6.35 (s, 1H), 6.87 (s, 1H), 8.50 (s, 1H), 9.49 (s, 1H), 9.52 (s, 1H). ^{13}C NMR (75 MHz, DMSO, δ ppm): 169.22, 161.20, 160.32, 157.21, 155.02 (2C), 133.44, 124.99,

117.98, 113.82, 104.51, 43.10, 41.16, 31.50, 27.99. IR (KBr): 3127, 2923, 2361, 1600, 1438, 1404, 1262, 1198, 1122, 1052, 908, 776, 737 cm^{-1}. HRMS (ESI): calcd for $C_{15}H_{14}ClN_3O_3$ $[M + H]^+$ 320.0724, found 320.0732. Purity: 97.36% by HPLC ($MeOH/H_2O$ = 80:20).

4.2. Computational method

4.2.1. Preparation of the active set, decoy set and the Topscience database

The Topscience database was downloaded from the official website (www.tsbiochem.com). Multiple conformations of the compounds in the active set, decoy set and the Topscience database were generated by using OMEGA (Open Eye Scientific Software) with the following parameters: number of allowed conformations (nconfs) = 400, Ewindow = 10 kcal/mol and root-mean-square distance (RMS) = 0.5 Å. The Merck Molecular Force Field 94 (MMFF94) was used during the conformation generation. Ewindow is the value used to discard high-energy conformations. The maximum allowed conformations per compound was set to 400 to ensure complete conformational coverage.

4.2.2. Creation of the ROCS model and the validation of the model

ROCS model was generated on the basis of the bound conformation of **AT-13387**, which was directly separated from the cocrystal structure downloaded from protein data bank (PDB, ID: 2XJX). The algorithm is based on the idea that the molecular shape of compounds is similar if the molecules overlay well and any volume mismatch is resulting from shape dissimilarity. ROCS maximize the rigid body overlap of the molecular Gaussian functions and therefore the shared volume between a query molecule and a conformation of a database molecule. For the superimposition of molecules, a smooth Gaussian function is used to represent the molecular volume. Subsequently, the overlay of the molecules is corrected by matching of chemical functionalities described by "Color Force Field", which can be used to measure chemical complementarity, and to refine shape based superpositions based on chemical similarity. The CFF is composed of SMARTS rules that determine chemical centers plus rules to determine how such centers interact. The color force fields in ROCS define six similar TYPE color force-fields. The types are hydrogen-bond donors, hydrogen-bond acceptors, hydrophobes, anions, cations, and rings. Finally, ROCS combines the volume matching and features overlay to describe the shape similarity. The angles of the key bonds in **AT-13387** were calculated in Discovery Studio.

4.2.3. Virtual screening of the topscience database

Virtual screenings were then performed based on the query model of **AT-13387** using ROCS. The parameters for the ROCS run were set as follow: rank by = combo and shape tanimoto, besthits = 1. During the screening, ROCS compares database compounds and **AT-13387** by aligning the compounds and calculating the similarities including their volumes and chemical features. The similarity is represented by a combo score, ranging from 0 to 2. If the combo score is close to 2, then the molecules have an excellent shape and chemical-feature match, while values close to 0 imply poor shape and chemical-feature similarities. Finally, 50 compounds were retained and purchased from Topscience database with purity > 95% (Liquid chromatography–mass spectrometry, LC–MS).

4.2.4. Molecular docking

The hit compounds from ROCS were saved as SD file and then imported to Discovery Studio (DS) 3.0. They were firstly ionized and prepared conformations by 'Prepare Ligands' protocol in DS at pH 7.0. Powell conjugate gradient algorithm was then applied for the minimization of the hit compounds (convergence criterion of 0.0005 kcal/mol/M, energy minimizations in 20,000 steps) in CHARMm force field. The molecular docking was carried out using GOLD 5.1. GOLD uses a powerful genetic algorithm (GA) method for conformation search and docking. As one of the most successful and widely used docking programs, GOLD was tested on a data set of over 300 complexes extracted from the Protein Data Bank (PDB) and succeeded in more than 70% cases in reproducing the bound conformation of the ligand obtained from experiment. In the present study, the Hsp90-ligand complex (PDB id: 2XJX) was download from PDB for docking studies. Residues around the original ligand (radius 7.5 Å) that completely covered the ATP binding site were defined as the binding site. Docking studies were performed using the standard default settings with 100 GA runs of molecules. For each GA run, a maximum of 125,000 operations were performed. Considering ligand flexibility, special care has been taken by including options such as flipping of ring corners, pyramidal nitrogens, amides, secondary and tertiary amines, rotation of carboxylate groups, as well as torsion angle distribution and post-process rotatable bonds as default. The annealing parameters were used as default. Hydrophobic fitting points were calculated to facilitate the correct starting orientation of the compound for docking by placing the hydrophobic atoms appropriately in the corresponding areas of the active site. Cutoff values of 3.0 Å for hydrogen bonds and 4.0 Å for van der Waals interactions were set. The docking was terminated when top ten solutions attained root-mean-square deviation (RMSD) values within 1.5 Å, The implemented scoring function Goldscore and Chemscore were used to consider the intra- and intermolecular hydrogen bonding interaction energy, van der Waals energy and ligand torsion energy.

4.3. Biology

4.3.1. Malachite green assay

The assay procedures were based on the literature [50]. The test compounds were diluted from mother plates (10 mM in 100% (v/v) DMSO) into daughter plates (200 μM in 2.0% (v/v) DMSO); 5 μL of test compound solution was added to each well (equivalent to a final concentration of 40 μM) of the 96-well assay plate. The first and last rows of the 96-well plate contained the appropriate concentration of DMSO were used as blank control. ATP was dissolved in the assay buffer to give a stock concentration of 2.5 mM and stored at room temperature. A 10 μL aliquot of ATP solution was added to each well to give a final assay concentration of 1 mM. Before the usage, Hsp90 protein was thawed on ice and suspended in chilled assay buffer to a stock concentration of 0.45 mg/mL, and the solution was kept on ice. The incubation was started by adding 10 μL of the stock Hsp90 to each well (except for the background wells which received 10 μL of assay buffer), giving a final assay volume of 25 μL. The plates were shaken for approximately 2 min and incubated for 3 h at 37 °C.

To stop the ATPase reactions, 10 μL of the Malachite green reagent A (Sciencell, 8118) was added to each well. Following the addition of 10 μL of Malachite green reagent B (Sciencell, 8118) to each well, the plate was incubated at room temperature for about 15 min, and the absorbance at 620 nm was measured by Varioskan Multimode Microplate Spectrophotometer (Thermo, Waltham, MA, USA).

4.3.2. The preparation of Hsp90 and measurement of ATP hydrolysis inhibition

The region encoding full-length Hsp90 was subcloned into pET28a. *Escherichia coli* cells with protein expression were induced with 0.5 mM IPTG. Cells were incubated at 16 °C for 20 h and then were harvested and disrupted by sonication. After centrifugation of

the soluble lysate, a Ni^{2+}-nitrilo-triacetic acid (NTA) agarose column in a buffer (50 mM Tris-Cl, 300 mM NaCl, 10 mM Imidazole, 10% [v/v] Glycerol, 10 mM PMSF, 10 mM DTT) was used for the separation of Hsp90, which was eluted with a linear gradient of 20–1000 mM imidazole. Hsp90 was identified by SDS-PAGE, and the high concentrated fraction was dialyzed against ATPase buffer (20 mM Tris-Cl, pH 7.5; 6 mM MgCl2; 20 mM KCl). It was then aliquoted, frozen in liquid nitrogen and stored at −80 °C.

The Hsp90 ATP hydrolysis inhibitory effects of the compounds were evaluated by using the Discover RX ADP Hunter™ Plus Assay kit (Discoverx, Fremont, CA) as reported previously.[53] Briefly, The test compounds were diluted to 200 μM in 2.0% (v/v) DMSO; 5 mL of test compound solution with different concentrations was added to each well of the 96-well assay plate. The first and last rows of the 96-well plate contained the appropriate concentration of DMSO were used as blank control. ATP was dissolved in the assay buffer to give a stock concentration of 2.5 mM and stored at room temperature. 10 μL aliquot of prepared ATP solution was added to each well to give a final assay concentration of 1 mM. Hsp90 protein was thawed on ice before usage and then suspended in chilled assay buffer to a stock concentration of 0.45 mg/mL. The incubation was started by adding 10 μL of the stock Hsp90 to each well (except for the background wells which received 10 μL of assay buffer), leading to a final assay volume of 25 μL and then incubated for 3 h at 37 °C. The Discover RX ADP Hunter™ Plus Assay kit was used for the detection of the ATP hydrolysis following the manufacturer's instructions. The concentration of ADP was measured using Varioskan spectrophotometer (Thermo, 540 nm excitation and 620 nm emission). Fluorescence intensity values measured for Hsp90 without any testing compound was assumed as 100% of enzyme activity. The background reaction rate was measured in a reaction lacking enzyme or substrate and subtracted from the experimental rates.

4.3.3. The fluorescence polarization (FP) competitive binding assay

Assays contained Hsp90/GA-FITC assay mix (100 mM Tris.Cl at pH 7.4, 20 mM KCl, 6 mM MgCl2, 5 μg/ml BSA, 10 nM Hsp90, 10 nM GA-FITC) and 2% DMSO as a vehicle for the compounds. Compounds were added to 384 well plates (Corning #3575) as 10-fold stocks in 5 μl of 20% DMSO/80% assay mix, then 45 μL of assay mix was added. After 30 min equilibration at room temperature in the dark, fluorescence polarization was measured using a Synergy plate reader (Molecular Devices SpectraMax Paradigm; Ex 485 nm, Em 535 nm). For this assay Z′ values were typically >0.8. IC50 were calculated using Graphpad Prims 5.

4.3.4. Anti-proliferation activity

Cell viabilities were determined by a colorimetric assay using 3-(4,5-dimethylthiaz-ol-2-yl)-2,5- diphenyltetrazoliumbromide (MTT, *Sigma*, *St. Louis*, *MO*) as described previously [51]. Cells that were given only culture media were used as control. After incubation for 48 h, absorbance (*A*) was measured at 570 nm. Survival ratio (%) was calculated as follow:

$$\text{Survival ratio}\ (\%) = (A_{\text{treatment}}/A_{\text{control}}) \times 100\%.$$

IC_{50} was taken as the concentration that caused 50% inhibition of cell viabilities and calculated by the Graphpad 5.0 software.

4.3.5. Hsp70 luciferase reporter assay of the hit compounds

HSPA1A promoter-driven luciferase plasmid was granted by Professor Jianhua Liu [52] and the methods have been described previously with little modification [53,54]. SK-BR-3 cells were grown in 24 well plates in 1640 containing sodium pyruvate 0.11 mg/mL, 10% FCS. The cells were co-transfected with pHSPA1A-Luc and pRL-SV40 (a plasmid encoding Renilla luciferase) by using lipofectamine and after 6 h the cells were treated with the indicated concentrations of the various compounds for 24 h. Luciferase activity was assessed by dual-luciferase reporter assay system (Promega, E1910) using a luminometer (Thermo Scientific Luminoskan Ascent). The level of HSP70 activation for a sample was calculated as the ratio between firefly and Renilla luciferase activity for the same sample. Typically, each sample was run in triplicate. Compounds giving firefly/Renilla luciferase ratios >1-fold higher than the corresponding ratios for the control samples (DMSO) were selected for retesting in a dose–response format, using the same assay. Results shown are from triplicate wells obtained in at least three separate experiments. Preliminary experiments validated that the reporter was strongly activated as expected by **AT-13387** (~5-fold).

4.3.6. Western-blot analysis

SK-Br-3 cells were pretreated with various concentrations of the test compounds. After stimulation, cells were collected; lysed in lysis buffer [50 mM Tris-Cl, pH 7.6, 150 Mm NaCl, 1 mM EDTA, 1% (m/v) Nonidet P-40 (NP-40), 0.2 mM Phenylmethanesulfonyl fluoride (PMSF), 0.1 mM NaF and 1.0 mM dithiothreitol (DTT)], and the supernatant was obtained after centrifugation at 13,000× g for 10 min at 4 °C. The concentration of protein in the supernatants was measured by the bicinchoninic acid (BCA) assay. Then equal amounts of protein (50 μg) were separated by 8% or 10% sodium dodecyl sulfate polyacrylamide gel electrophoresis (SDS-PAGE) and transferred onto the PVDF membranes (Millipore, Billerica, MA). The blots were incubated with specific antibodies against the indicated primary antibodies overnight at 4 °C followed by IRDyeTM800-conjugated secondary antibody for 1 h at 37 °C. Detection was performed by the Odyssey Infrared Imaging System (LI-COR; Lincoln, NE). All blots were stripped and incubated with polyclonal anti-β-actin antibody to ascertain equal loading of proteins.

Acknowledgments

This work was supported by the grants from the National Natural Science Foundation of China (No. 81230078 (key program), 81202463 (youth foundation) and 91129732 (general program)), the grant from the National High Technology Research and Development Program of China (863 Program, No. 2012AA020301) and the grants from National Major Science and Technology Project of China (Innovation and Development of New Drugs, No. 2010ZX09401-401 and 2009ZX09501-003). The authors declare no other conflicts of interest.

Appendix A. Supplementary data

Supplementary data related to this article can be found at http://dx.doi.org/10.1016/j.ejmech.2014.03.061.

References

[1] C. Jolly, R.I. Morimoto, Journal of the National Cancer Institute 92 (2000) 1564–1572.
[2] J.D. West, Y. Wang, K.A. Morano, Chemical Research in Toxicology 25 (2012) 2036–2053.
[3] Y.M. Xu, D.Y. Huang, J.F. Chiu, A.T. Lau, Journal of Proteome Research 11 (2012) 2625–2634.
[4] Y.L. Janin, Drug Discovery Today 15 (2010) 342–353.
[5] A. Maloney, P. Workman, Expert Opinion on Biological Therapy 2 (2002) 3–24.
[6] L.H. Pearl, C. Prodromou, Annual Review of Biochemistry 75 (2006) 271–294.
[7] J. Trepel, M. Mollapour, G. Giaccone, L. Neckers, Nature Reviews Cancer 10 (2010) 537–549.

[8] H. Hao, Y. Naomoto, X. Bao, N. Watanabe, K. Sakurama, K. Noma, T. Motoki, Y. Tomono, T. Fukazawa, Y. Shirakawa, T. Yamatsuji, J. Matsuoka, M. Takaoka, Oncology Reports 23 (2010) 1483–1492.
[9] A. Kamal, M.F. Boehm, F.J. Burrows, Trends in Molecular Medicine 10 (2004) 283–290.
[10] S. Messaoudi, J.F. Peyrat, J.D. Brion, M. Alami, Anti-Cancer Agents in Medicinal Chemistry 8 (2008) 761–782.
[11] W.B. Pratt, Y. Morishima, H.M. Peng, Y. Osawa, Experimental Biology and Medicine (Maywood) 235 (2010) 278–289.
[12] J.S. Isaacs, W. Xu, L. Neckers, Cancer Cell 3 (2003) 213–217.
[13] D.J. Stravopodis, L.H. Margaritis, G.E. Voutsinas, Current Medicinal Chemistry 14 (2007) 3122–3138.
[14] L. Whitesell, S.L. Lindquist, Nature Reviews Cancer 5 (2005) 761–772.
[15] D. Picard, Cellular and Molecular Life Sciences 59 (2002) 1640–1648.
[16] A. Kamal, L. Thao, J. Sensintaffar, L. Zhang, M.F. Boehm, L.C. Fritz, F.J. Burrows, Nature 425 (2003) 407–410.
[17] K. Moulick, J.H. Ahn, H. Zong, A. Rodina, L. Cerchietti, E.M. Gomes DaGama, E. Caldas-Lopes, K. Beebe, F. Perna, K. Hatzi, L.P. Vu, X. Zhao, D. Zatorska, T. Taldone, P. Smith-Jones, M. Alpaugh, S.S. Gross, N. Pillarsetty, T. Ku, J.S. Lewis, S.M. Larson, R. Levine, H. Erdjument-Bromage, M.L. Guzman, S.D. Nimer, A. Melnick, L. Neckers, G. Chiosis, Nature Chemical Biology 7 (2011) 818–826.
[18] J. Shi, R. Van de Water, K. Hong, R.B. Lamer, K.W. Weichert, C.M. Sandoval, S.R. Kasibhatla, M.F. Boehm, J. Chao, K. Lundgren, N. Timple, R. Lough, G. Ibanez, C. Boykin, F.J. Burrows, M.R. Kehry, T.J. Yun, E.K. Harning, C. Ambrose, J. Thompson, S.A. Bixler, A. Dunah, P. Snodgrass-Belt, J. Arndt, I.J. Enyedy, P. Li, V.S. Hong, A. McKenzie, M.A. Biamonte, Journal of Medicinal Chemistry 55 (2012) 7786–7795.
[19] L. Neckers, Current Medicinal Chemistry 10 (2003) 733–739.
[20] P. Workman, Cancer Letters 206 (2004) 149–157.
[21] L. Whitesell, S.D. Shifrin, G. Schwab, L.M. Neckers, Cancer Research 52 (1992) 1721–1728.
[22] R.C. Schnur, M.L. Corman, R.J. Gallaschun, B.A. Cooper, M.F. Dee, J.L. Doty, M.L. Muzzi, C.I. DiOrio, E.G. Barbacci, P.E. Miller, et al., Journal of Medicinal Chemistry 38 (1995) 3813–3820.
[23] E.R. Glaze, A.C. Smith, D.W. Johnson, D.L. McCormick, A.B. Brown, B.S. Levin, R. Krishnaraj, A. Lyubimov, M.J. Egorin, J.E. Tomaszewski, Cancer Research 44 (2003), 162–162.
[24] J. Ge, E. Normant, J.R. Porter, J.A. Ali, M.S. Dembski, Y. Gao, A.T. Georges, L. Grenier, R.H. Pak, J. Patterson, J.R. Sydor, T.T. Tibbitts, J.K. Tong, J. Adams, V.J. Palombella, Journal of Medicinal Chemistry 49 (2006) 4606–4615.
[25] L.V. Sequist, S. Gettinger, N.N. Senzer, R.G. Martins, P.A. Janne, R. Lilenbaum, J.E. Gray, A.J. Iafrate, R. Katayama, N. Hafeez, J. Sweeney, J.R. Walker, C. Fritz, R.W. Ross, D. Grayzel, J.A. Engelman, D.R. Borger, G. Paez, R. Natale, Journal of Clinical Oncology 28 (2010) 4953–4960.
[26] M.A. Biamonte, R. Van de Water, J.W. Arndt, R.H. Scannevin, D. Perret, W.C. Lee, Journal of Medicinal Chemistry 53 (2010) 3–17.
[27] J.M. Holzbeierlein, A. Windsperger, G. Vielhauer, Current Oncology Reports 12 (2010) 95–101.
[28] H. He, D. Zatorska, J. Kim, J. Aguirre, L. Llauger, Y. She, N. Wu, R.M. Immormino, D.T. Gewirth, G. Chiosis, Journal of Medicinal Chemistry 49 (2006) 381–390.
[29] (a) R.M. Immormino, Y. Kang, G. Chiosis, D.T. Gewirth, Journal of Medicinal Chemistry 49 (2006) 4953–4960;
(b) E. Caldas-Lopes, L. Cerchietti, J.H. Ahn, C.C. Clement, A.I. Robles, A. Rodina, K. Moulick, T. Taldone, A. Gozman, Y. Guo, N. Wu, E. de Stanchina, J. White, S.S. Gross, Y. Ma, L. Varticovski, A. Melnick, G. Chiosis, Proceedings of the National Academy of Sciences of the United States of America 106 (2009) 8368–8373.
[30] R. Bao, C.J. Lai, H. Qu, D. Wang, L. Yin, B. Zifcak, R. Atoyan, J. Wang, M. Samson, J. Forrester, S. DellaRocca, G.X. Xu, X. Tao, H.X. Zhai, X. Cai, C. Qian, Clinical Cancer Research 15 (2009) 4046–4057.
[31] D. Papac, J.S. Patton, L. Reeves, L. DeMie, C. Bradford, B. Hachey, B. Clemetson, C. Christensen, S.H. Kim, R. Tangallapally, D. Parker, R. Trovato, I.C. Kim, D. Wettstein, V.R. Baichwal, A. Bajji, Cancer Research 71 (2011) 3237–3245.
[32] S.R. Kasibhatla, K. Hong, M.A. Biamonte, D.J. Busch, P.L. Karjian, J.L. Sensintaffar, A. Kamal, R.E. Lough, J. Brekken, K. Lundgren, R. Grecko, G.A. Timony, Y. Ran, R. Mansfield, L.C. Fritz, E. Ulm, F.J. Burrows, M.F. Boehm, Journal of Medicinal Chemistry 50 (2007) 2767–2778.
[33] P.A. Brough, W. Aherne, X. Barril, J. Borgognoni, K. Boxall, J.E. Cansfield, K.M. Cheung, I. Collins, N.G. Davies, M.J. Drysdale, B. Dymock, S.A. Eccles, H. Finch, A. Fink, A. Hayes, R. Howes, R.E. Hubbard, K. James, A.M. Jordan, A. Lockie, V. Martins, A. Massey, T.P. Matthews, E. McDonald, C.J. Northfield, L.H. Pearl, C. Prodromou, S. Ray, F.I. Raynaud, S.D. Roughley, S.Y. Sharp, A. Surgenor, D.L. Walmsley, P. Webb, M. Wood, P. Workman, L. Wright, Journal of Medicinal Chemistry 51 (2008) 196–218.
[34] A.J. Woodhead, H. Angove, M.G. Carr, G. Chessari, M. Congreve, J.E. Coyle, J. Cosme, B. Graham, P.J. Day, R. Downham, L. Fazal, R. Feltell, E. Figueroa, M. Frederickson, J. Lewis, R. McMenamin, C.W. Murray, M.A. O'Brien, L. Parra, S. Patel, T. Phillips, D.C. Rees, S. Rich, D.M. Smith, G. Trewartha, M. Vinkovic, B. Williams, A.J. Woolford, Journal of Medicinal Chemistry 53 (2010) 5956–5969.
[35] W. Ying, Z. Du, L. Sun, K.P. Foley, D.A. Proia, R.K. Blackman, D. Zhou, T. Inoue, N. Tatsuta, J. Sang, S. Ye, J. Acquaviva, L.S. Ogawa, Y. Wada, J. Barsoum, K. Koya, Molecular Cancer Therapeutics 11 (2012) 475–484.
[36] T. Nakashima, T. Ishii, H. Tagaya, T. Seike, H. Nakagawa, Y. Kanda, S. Akinaga, S. Soga, Y. Shiotsu, Clinical Cancer Research 16 (2010) 2792–2802.
[37] Combination of ligand- and structure-based methods in virtual screening, Drug Discovery Today: Technologies 10 (3) (2013 Sep) e395–401, http://dx.doi.org/10.1016/j.ddtec.2013.02.002.
[38] T. Scior, A. Bender, G. Tresadern, J.L. Medina-Franco, K. Martínez-Mayorga, T. Langer, K. Cuanalo-Contreras, D.K. Agrafiotis, Recognizing pitfalls in virtual screening: a critical review, Journal of Chemical Information and Modeling 52 (4) (2012 Apr 23) 867–881, http://dx.doi.org/10.1021/ci200528d. Epub 2012 Apr 6.
[39] A. Lavecchia, C. Di Giovanni, Virtual screening strategies in drug discovery: a critical review, Current Medicinal Chemistry 20 (23) (2013) 2839–2860.
[40] P. Purushottamachar, A. Khandelwal, P. Chopra, N. Maheshwari, L.K. Gediya, T.S. Vasaitis, R.D. Bruno, O.O. Clement, V.C. Njar, Bioorganic & Medicinal Chemistry 15 (2007) 3413–3421.
[41] E. Sala, L. Guasch, J. Iwaszkiewicz, M. Mulero, M.J. Salvado, C. Blade, M. Ceballos, C. Valls, V. Zoete, A. Grosdidier, S. Garcia-Vallve, O. Michielin, G. Pujadas, European Journal of Medicinal Chemistry 46 (2011) 6098–6103.
[42] ROCS, 3.1.2; OpenEye Scientific Software: Santa Fe, NM, 2012.
[43] J.A. Grant, M.A. Gallardo, B.T. Pickup, Journal of Computational Chemistry 17 (1996) 1653–1666.
[44] D. Schuster, M. Spetea, M. Music, S. Rief, M. Fink, J. Kirchmair, J. Schutz, G. Wolber, T. Langer, H. Stuppner, H. Schmidhammer, J.M. Rollinger, Bioorganic & Medicinal Chemistry 18 (2010) 5071–5080.
[45] P.C.D. Hawkins, A.G. Skillman, A. Nicholls, Journal of Medicinal Chemistry 50 (2006) 74–82.
[46] C.W. Murray, M.G. Carr, O. Callaghan, G. Chessari, M. Congreve, S. Cowan, J.E. Coyle, R. Downham, E. Figueroa, M. Frederickson, B. Graham, R. McMenamin, M.A. O'Brien, S. Patel, T.R. Phillips, G. Williams, A.J. Woodhead, A.J.A. Woolford, Journal of Medicinal Chemistry 53 (2010) 5942–5955.
[47] E.B. Cogan, G.B. Birrell, O.H. Griffith, Analytical Biochemistry 271 (1999) 29–35.
[48] J. Rumsfeld, K. Ziegelbauer, F. Spaltmann, Protein Expression and Purification 18 (2000) 303–309.
[49] S.M. Roe, C. Prodromou, R. O'Brien, J.E. Ladbury, P.W. Piper, L.H. Pearl, Journal of Medicinal Chemistry 42 (1999) 260–266.
[50] M.G. Rowlands, Y.M. Newbatt, C. Prodromou, L.H. Pearl, P. Workman, W. Aherne, Analytical Biochemistry 327 (2004) 176–183.
[51] J. Jia, X. Xu, F. Liu, X. Guo, M. Zhang, M. Lu, L. Xu, J. Wei, J. Zhu, S. Zhang, S. Zhang, H. Sun, Q. You, PLoS One 8 (2013) e59315.
[52] Y. Zheng, V. Le, Z. Cheng, S. Xie, H. Li, J. Tian, J. Liu, Cell Stress & Chaperones 18 (2013) 203–213.
[53] L. Xin, X. Li, H. Deng, D. Kuang, X. Dai, S. Huang, F. Wang, M. He, R.W. Currie, T. Wu, Cell Stress & Chaperones 17 (2012) 567–576.
[54] B.R. Kusuma, L. Zhang, T. Sundstrom, L.B. Peterson, R.T. Dobrowsky, B.S. Blagg, Journal of Medicinal Chemistry 55 (2012) 5797–5812.